Highly selective and sensitive colorimetric chemosensors for Hg^{2+} based on novel diaminomaleonitrile derivatives

Yanping Huo [a, b,*], Songying Wang [a], Tianhua Lu [a], Chengqiang Pan [a], Yujing Lu [a], Xianghua Yang [a], Dongping Hu [a], Sheng Hu [a]

[a] *School of Chemical Engineering and Light Industry, Guangdong University of Technology, Guangzhou 510006, China*

[b] *Key laboratory of Organofluorine Chemistry, Shanghai Institute of Organic Cheimstry, Chinese Academy of Sciences, Shanghai 200032, China*

*E-mail: yphuo@gdut.edu.cn(Y.-P. Huo);

Contents:

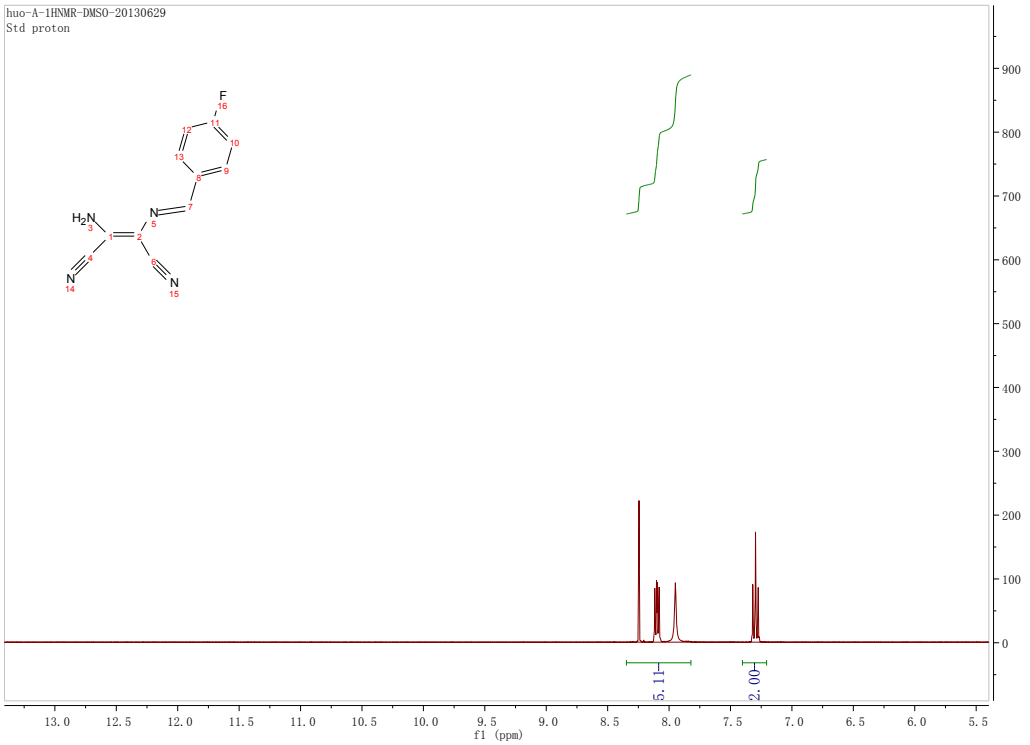

Figure S1. ^{1}H NMR of **A1**

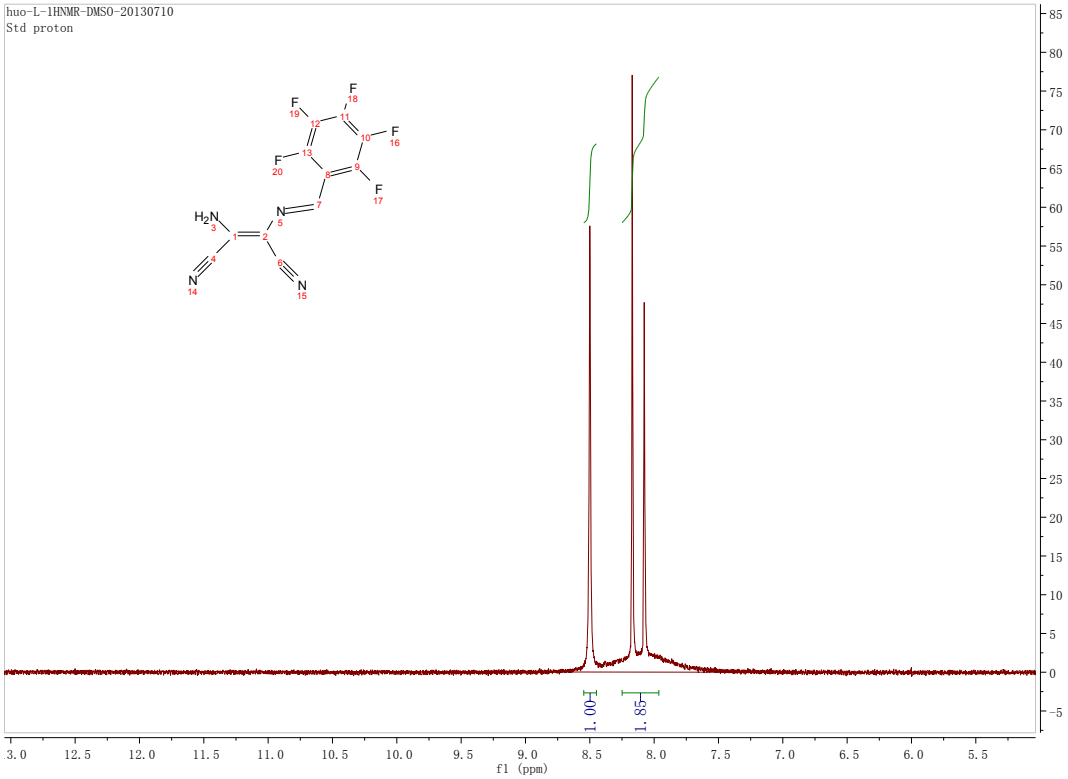

Figure S2. ^{1}H NMR of **A2**

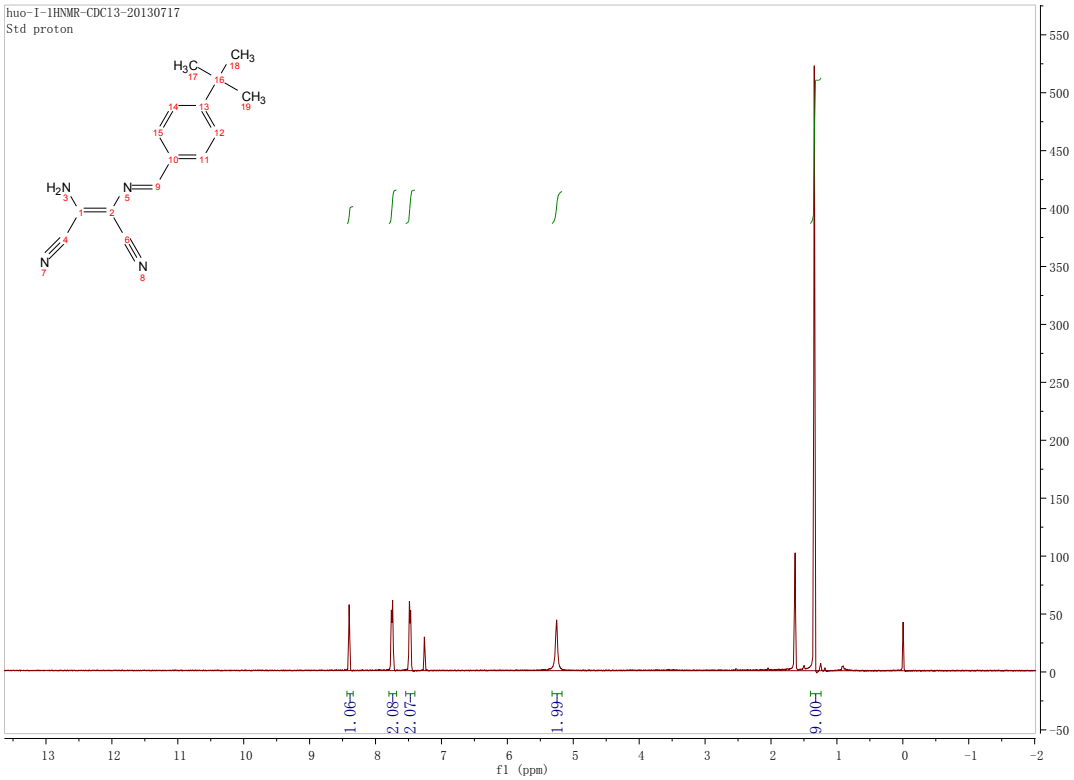

Figure S3. ^{1}H NMR of **A3**

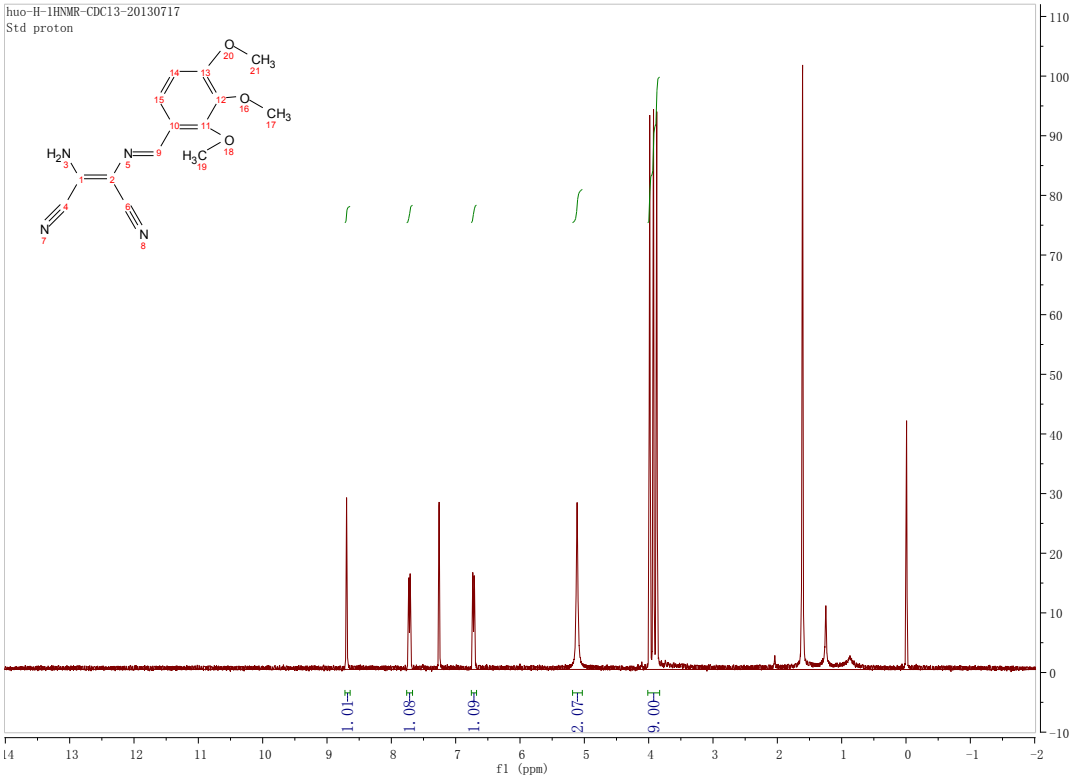

Figure S4. ^{1}H NMR of **A4**

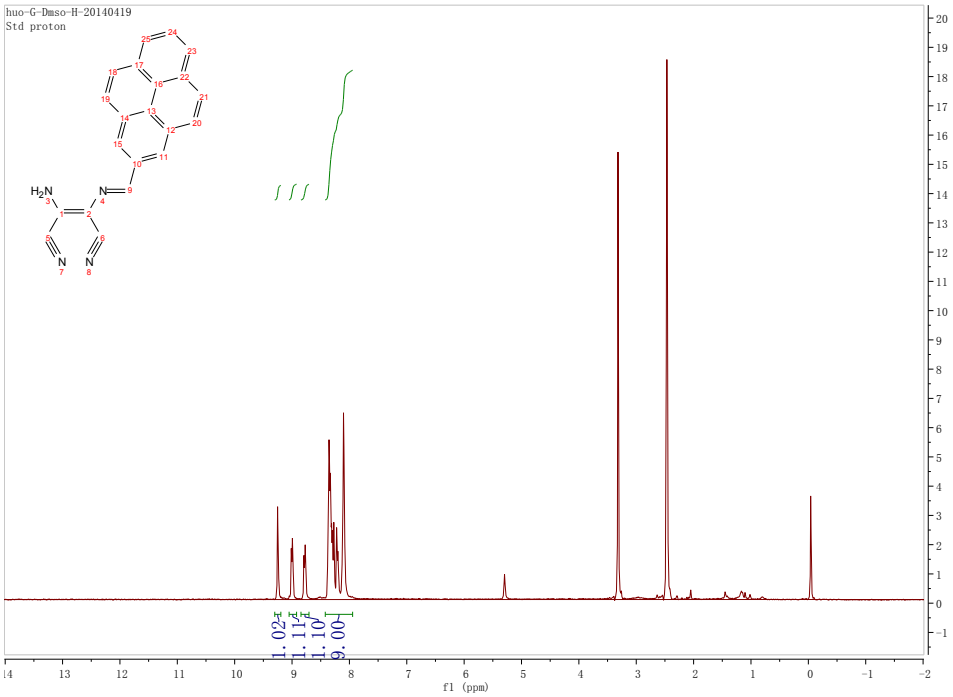

Figure S5. ^{1}H NMR of **A5**

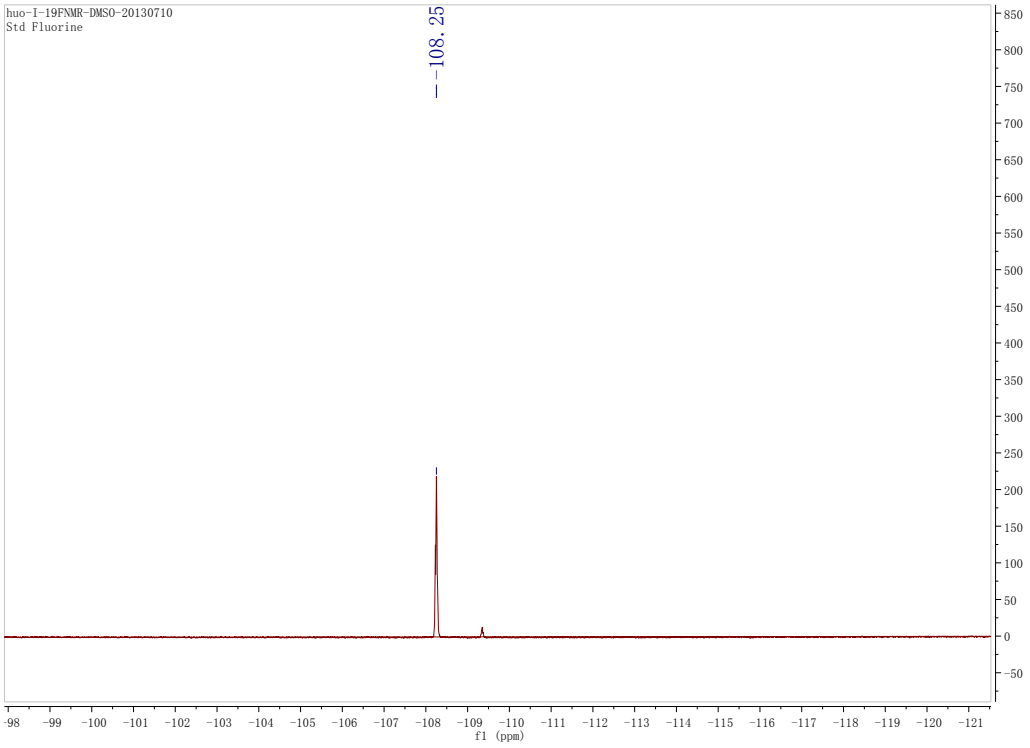

Figure S6. ^{19}F NMR of **A1**

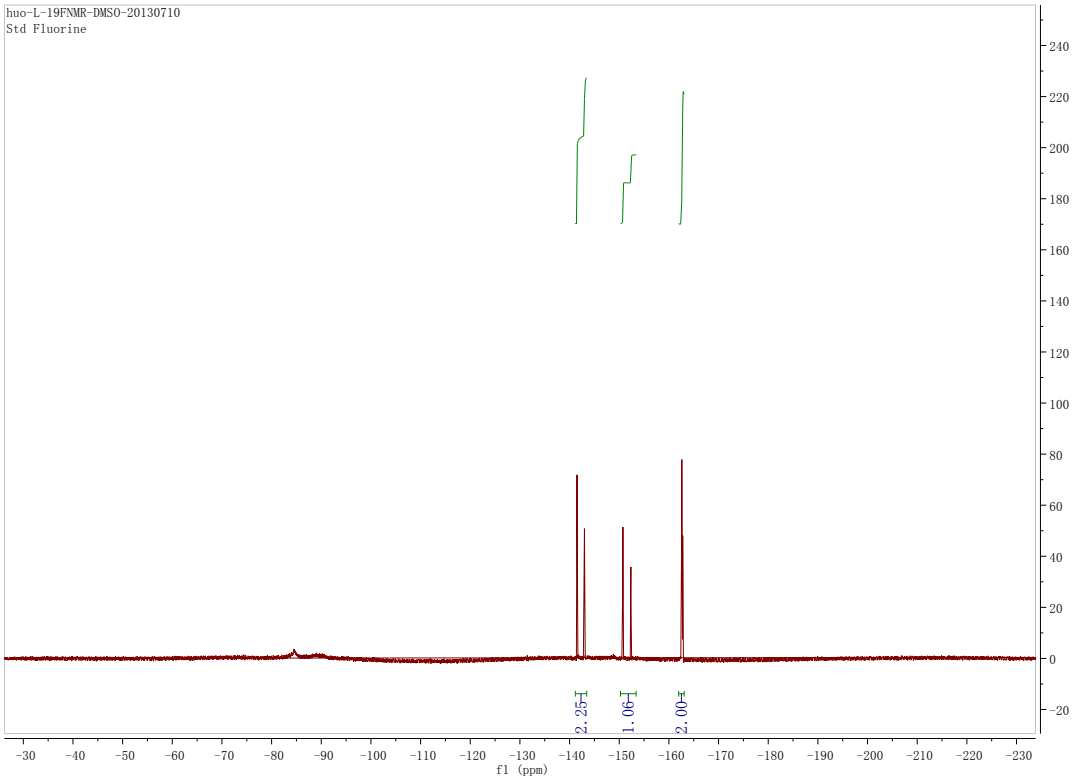

Figure S7. ^{19}F NMR of **A2**

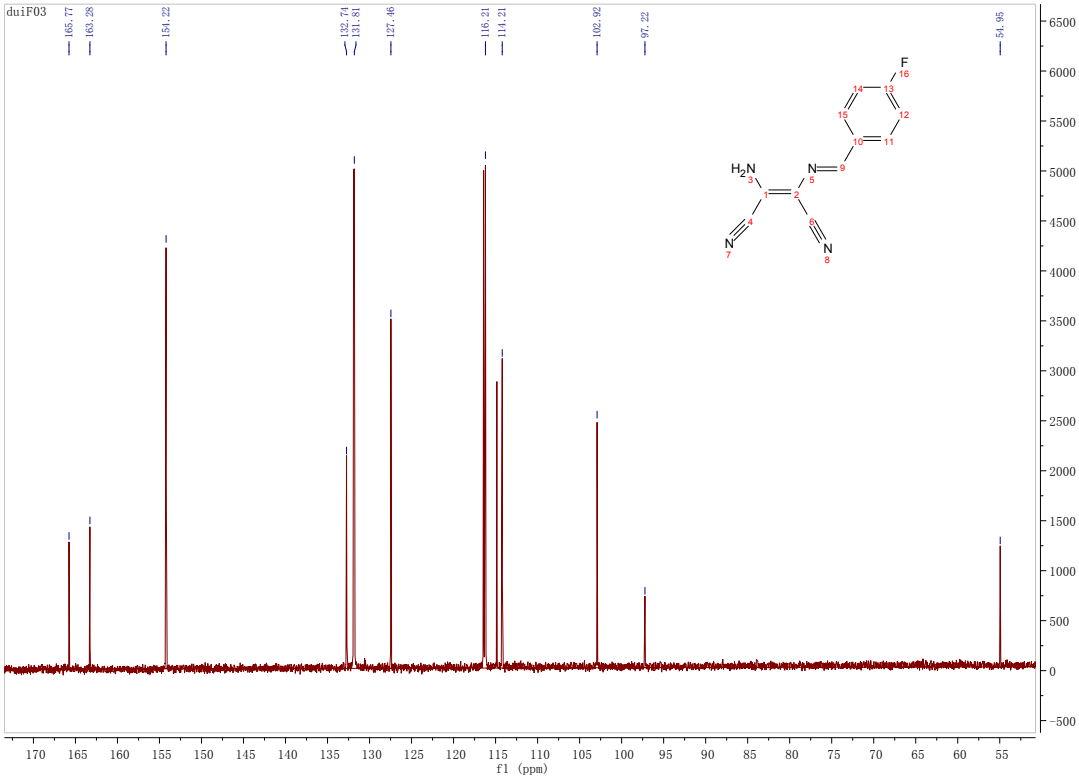

Figure S8. ^{13}C NMR of **A1**

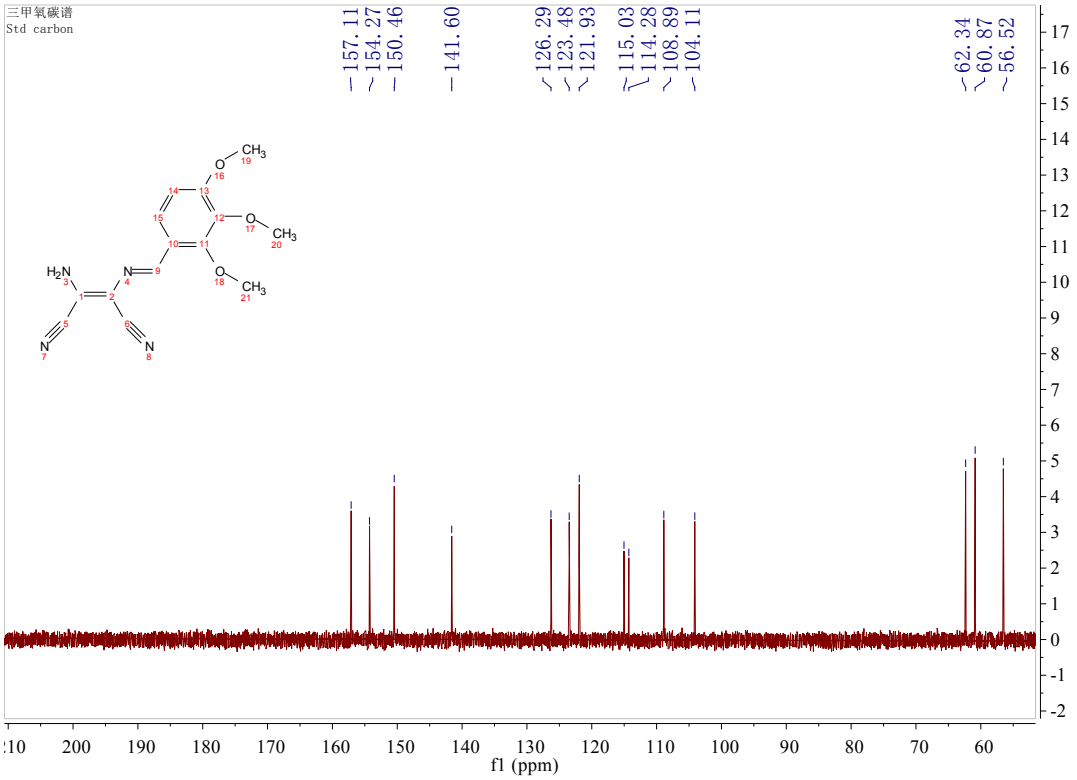

Figure S9. ^{13}C NMR of **A4**

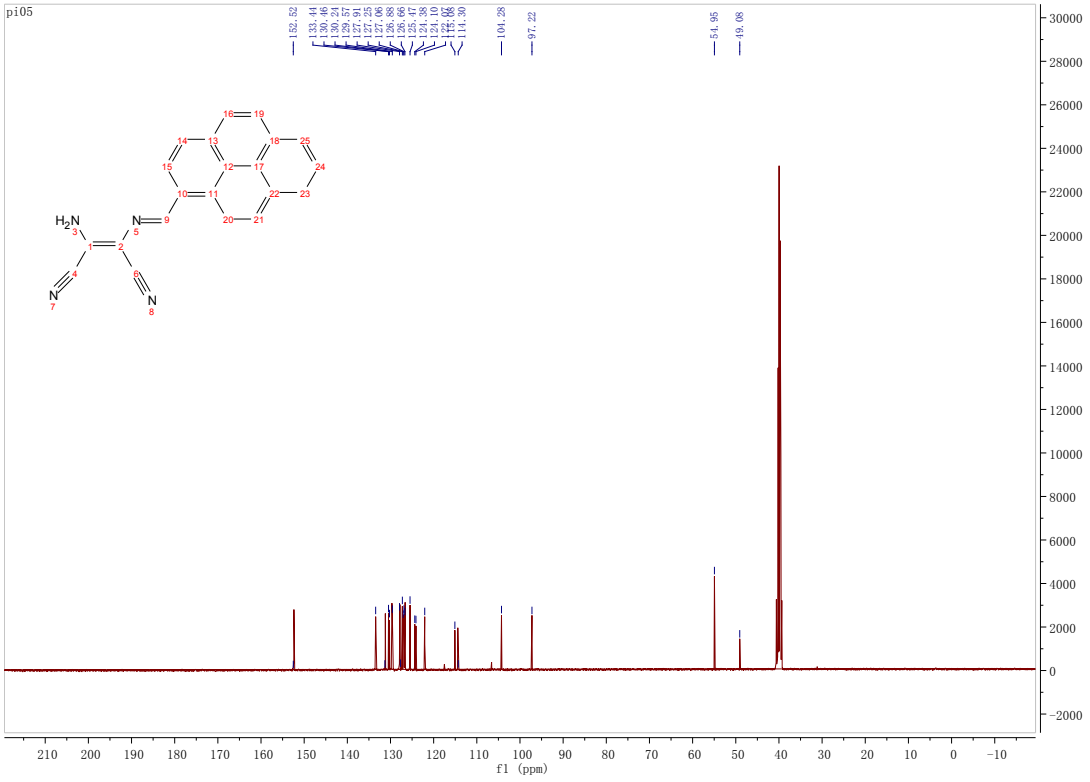

Figure S10. ^{13}C NMR of **A5**

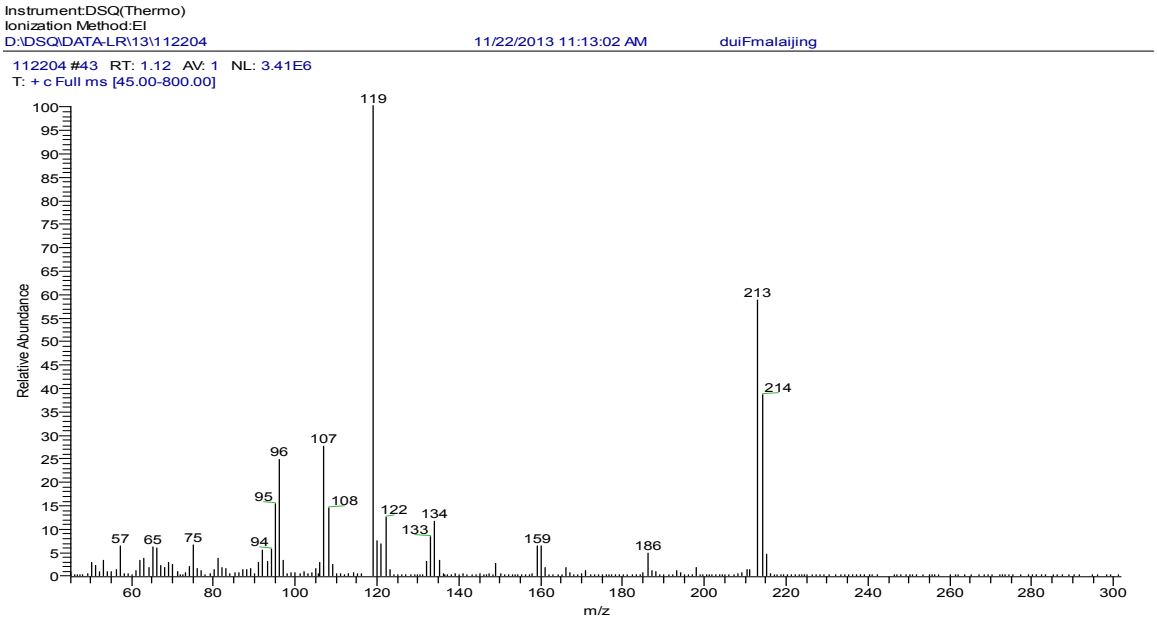

Figure S11. EI mass spectrum of **A1**

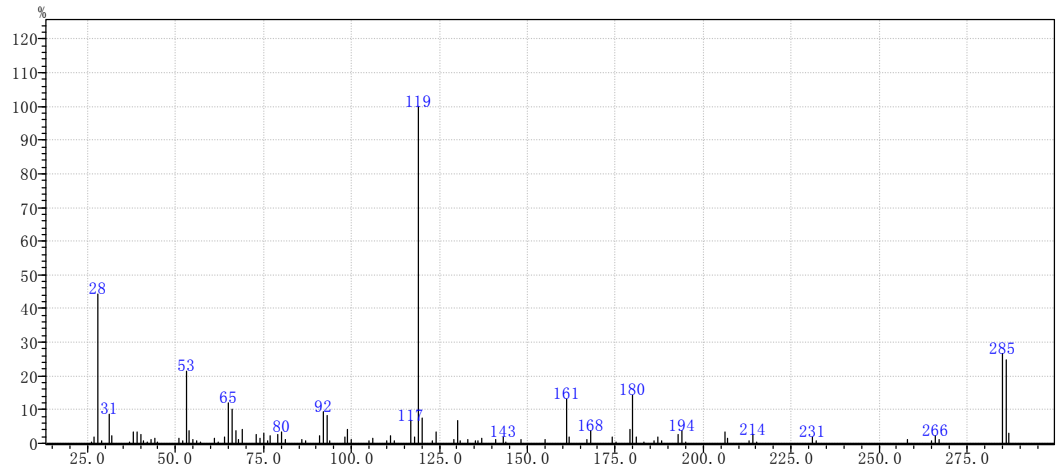

Figure S12. EI mass spectrum of **A2**

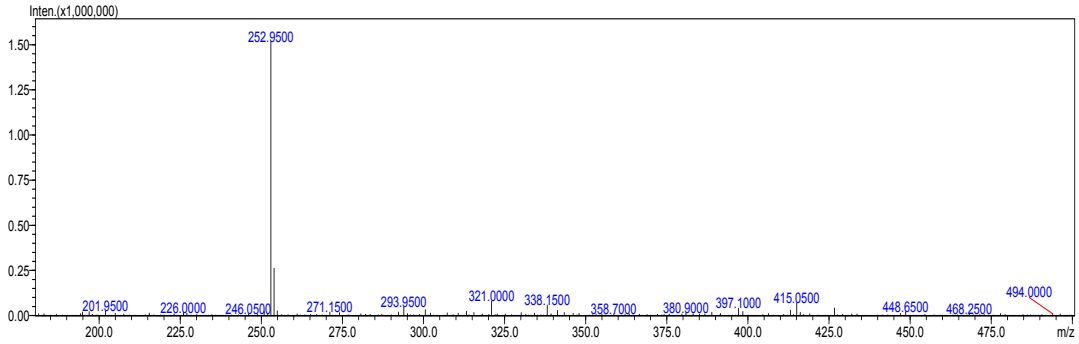

Figure S13. ESI mass spectrum of **A3**

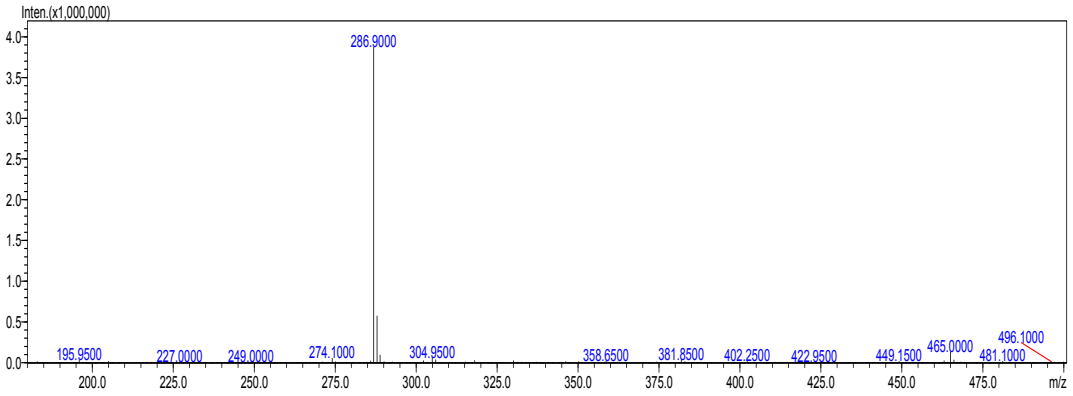

Figure S14. ESI mass spectrum of **A4**

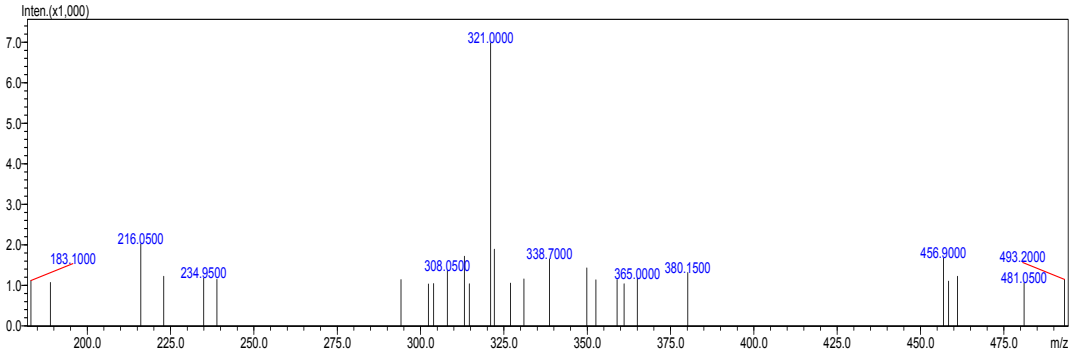

Figure S15. ESI mass spectrum of **A5**

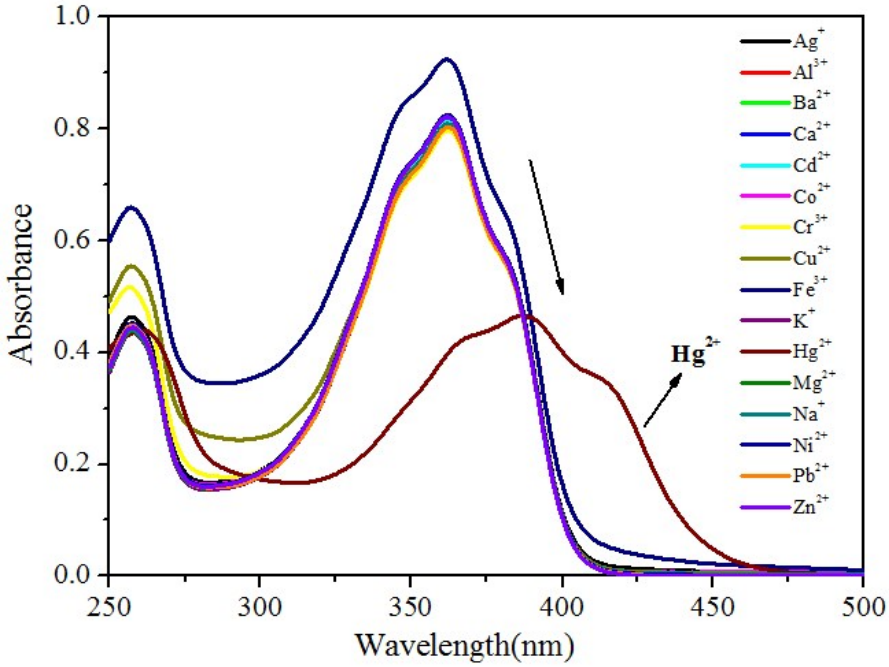

Figure S16. Absorption changes of **A1** in EtOH/H_2O (v/v = 4:1, 1.0 × 10^{-5} M) upon addition of 1 equiv of different nitrate salts(1.0 × 10^{-5} M).

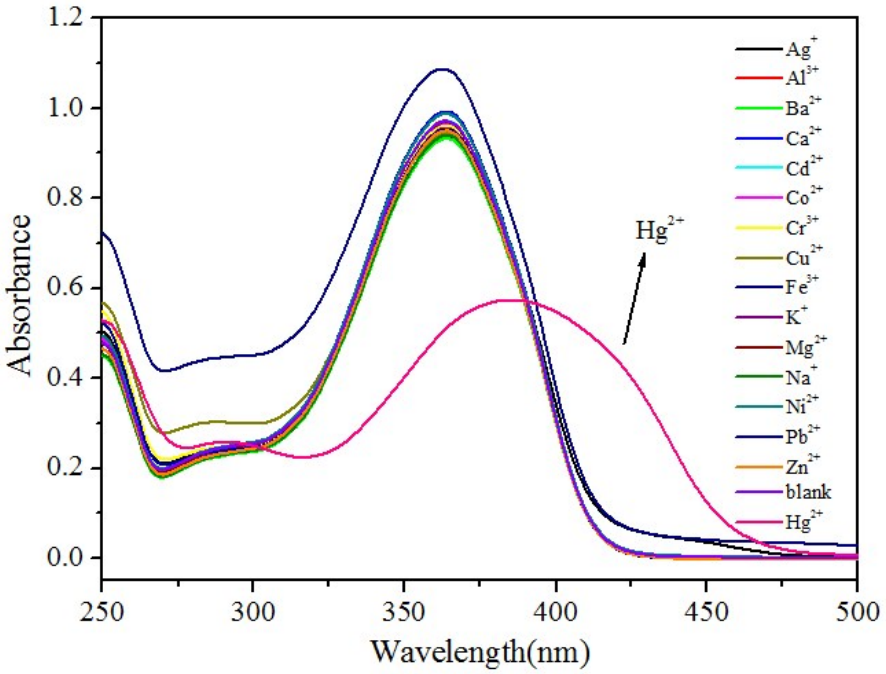

Figure S17. UV-vis responses of **A2** to various metal ions in EtOH/H_2O (v/v = 4:1).

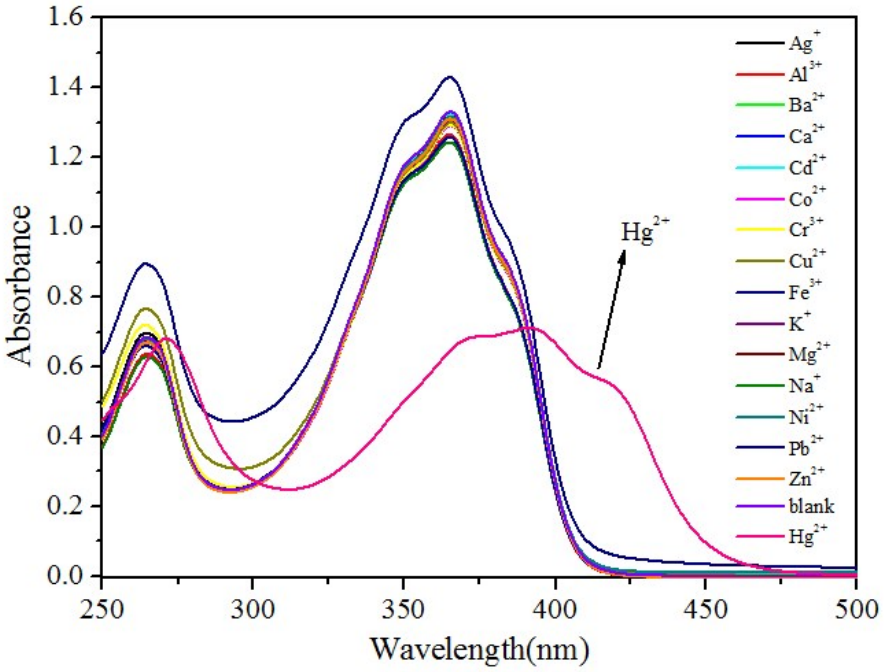

Figure S18. UV-vis responses of **A3** to various metal ions in EtOH/H_2O (v/v = 4:1).

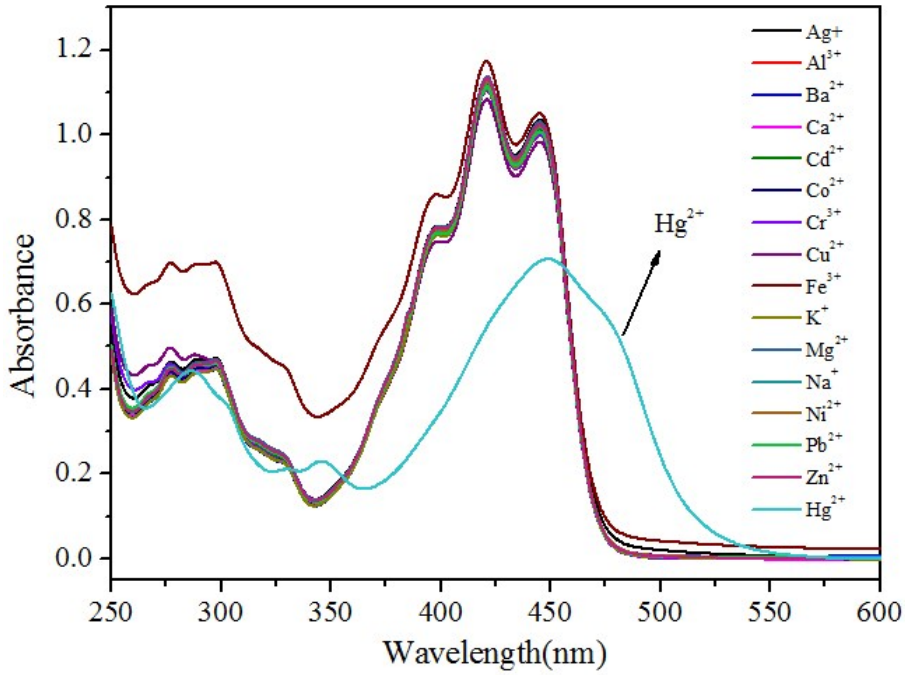

Figure S19. UV-vis responses of **A5** to various metal ions in EtOH/H_2O(v/v = 4:1).

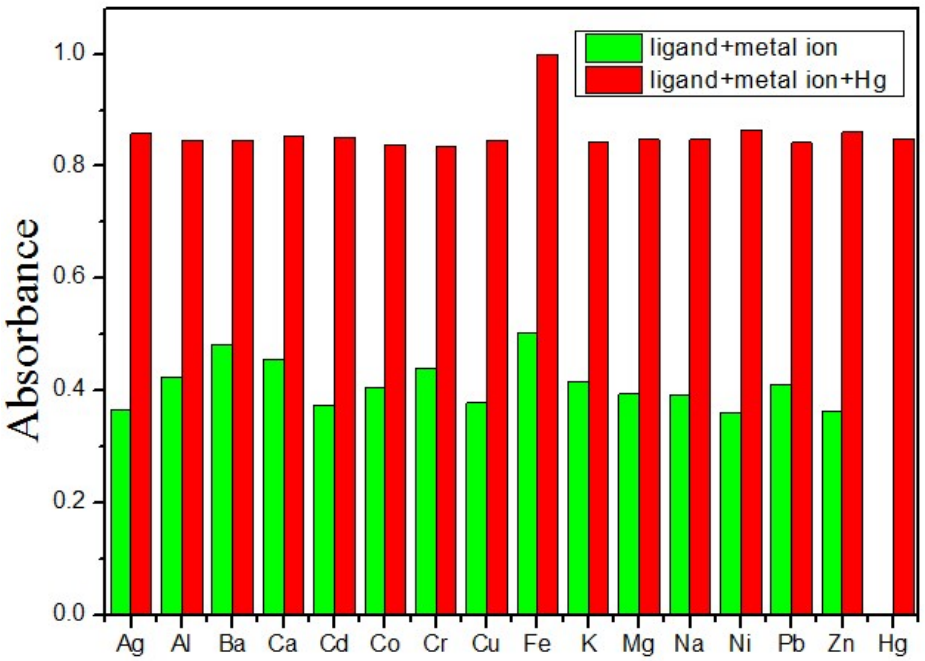

Figure S20**.** Absorbance of **A1**–Hg^{2+} at the new band upon addition of various cations. The low bars represent **A1** (1.0×10^{-5} M) with cations (5.0×10^{-5} M) without Hg^{2+}; the high bars represent **A1** (1.0×10^{-5} M) with cations (5.0×10^{-5} M) upon the subsequent addition of Hg^{2+} (1.0×10^{-5} M) in EtOH/H_2O(v/v = 4:1).

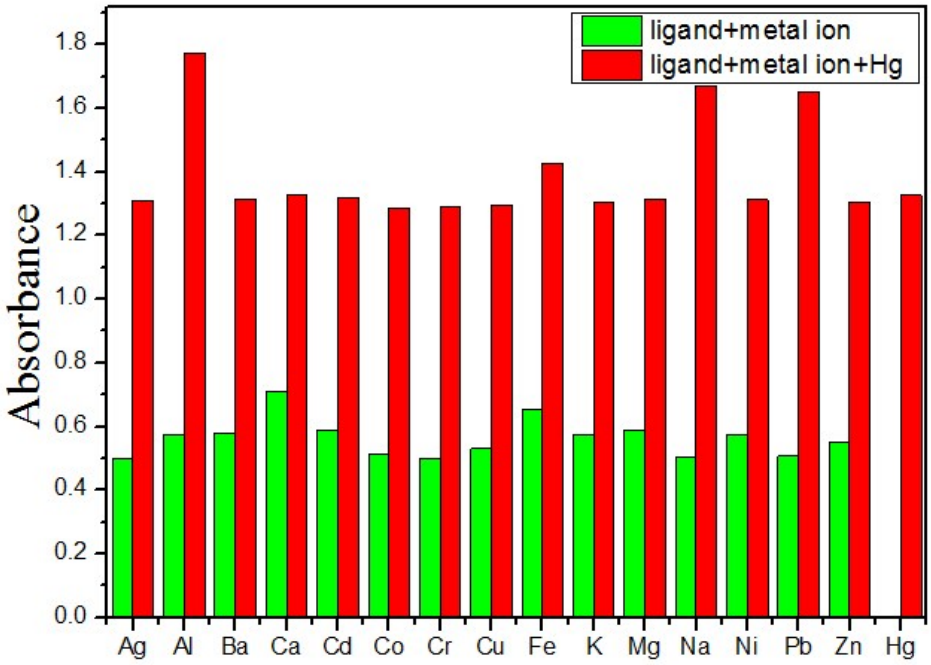

Figure S21. Absorbance of **A3**–Hg^{2+} at the new band upon addition of various cations. The low bars represent **A3** (1.0×10^{-5} M) with cations (5.0×10^{-5} M) without Hg^{2+}; the high bars represent **A3** (1.0×10^{-5} M) with cations (5.0×10^{-5} M) upon the subsequent addition of Hg^{2+} (1.0×10^{-5} M) in EtOH/H_2O(v/v = 4:1).

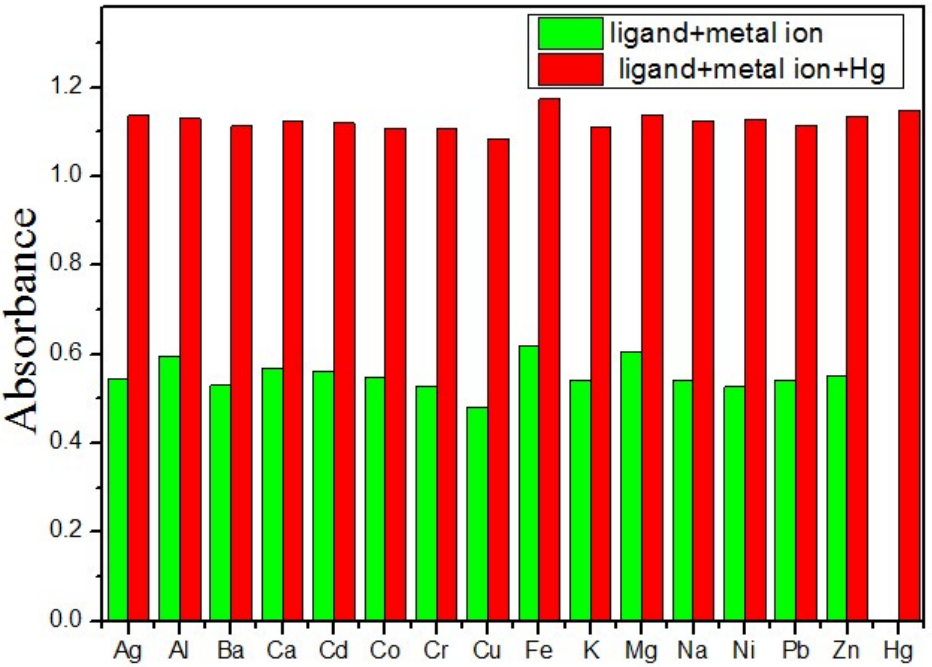

Figure S22. Absorbance of **A5**–Hg^{2+} at the new band upon addition of various cations. The low bars represent **A5** (1.0×10^{-5} M) with cations (5.0×10^{-5} M) without Hg^{2+}; the high bars represent **A5** (1.0×10^{-5} M) with cations (5.0×10^{-5} M) upon the subsequent addition of Hg^{2+} (1.0×10^{-5} M) in EtOH/H_2O(v/v = 4:1).

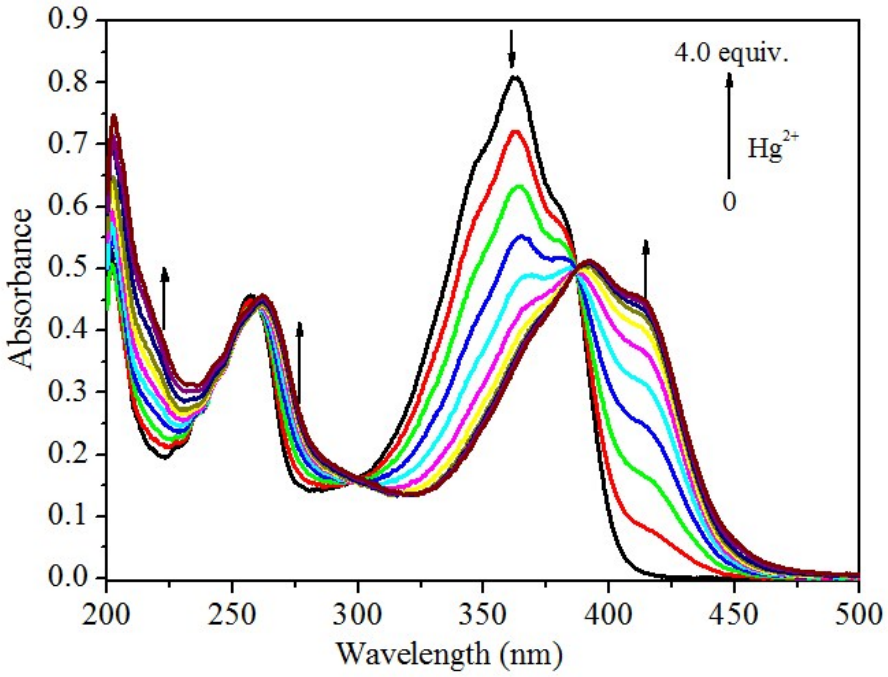

Fig. S23. Titration curves of **A1** in EtOH/H_2O(v/v = 4:1) in the presence of different amounts of Hg^{2+}.

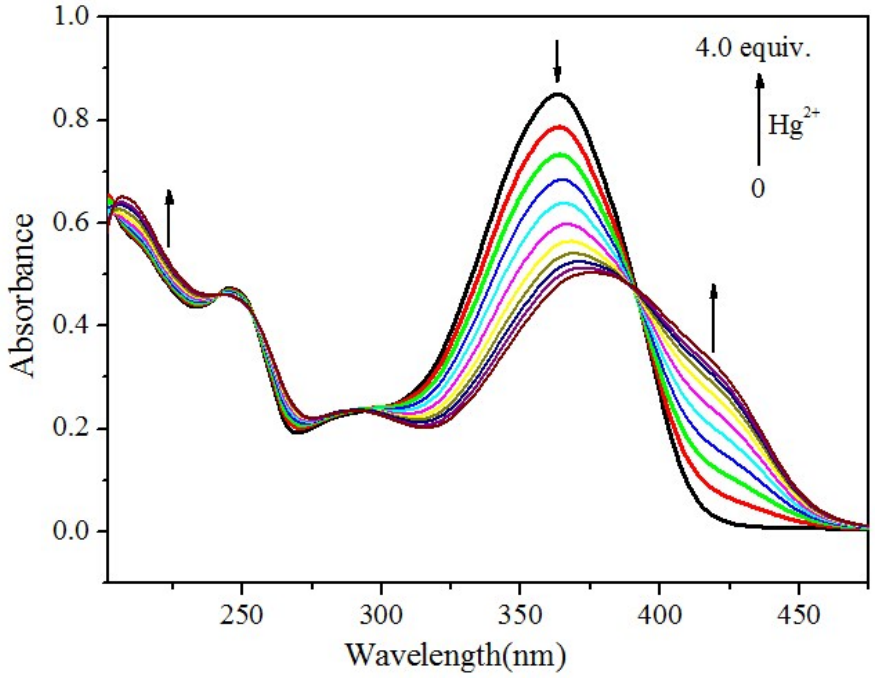

Figure S24. Titration curves of **A2** (1.0×10^{-5} M) in EtOH/H_2O (v/v = 4:1, 20mM HEPES buffer, pH=7.0) in the addition of 0.5 equimolar per drop.

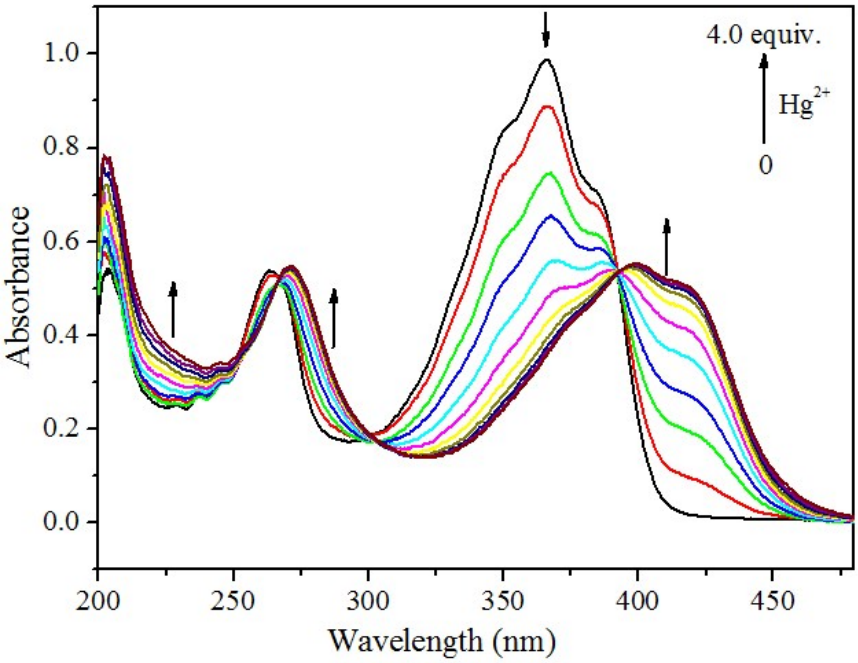

Figure S25. Titration curves of **A3** (1.0×10^{-5} M) in EtOH/H_2O (v/v = 4:1, 20 mM HEPES buffer, pH=7.0) in the addition of 0.5 equimolar per drop.

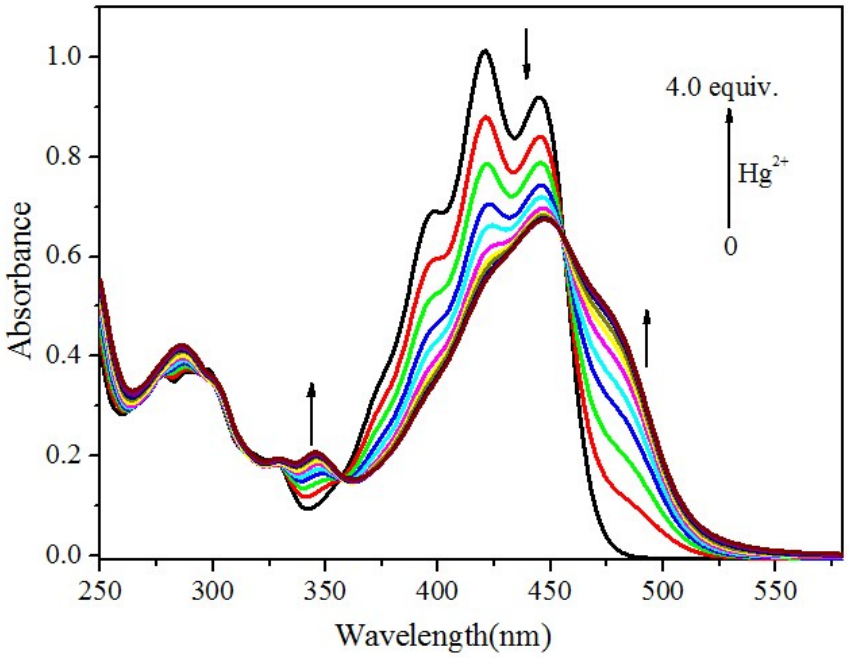

Figure S26. Titration curves of **A5** (1.0×10^{-5} M) in EtOH/H_2O (v/v = 4:1, 20 mM HEPES buffer, pH=7.0) in the addition of 0.5 equimolar per drop.

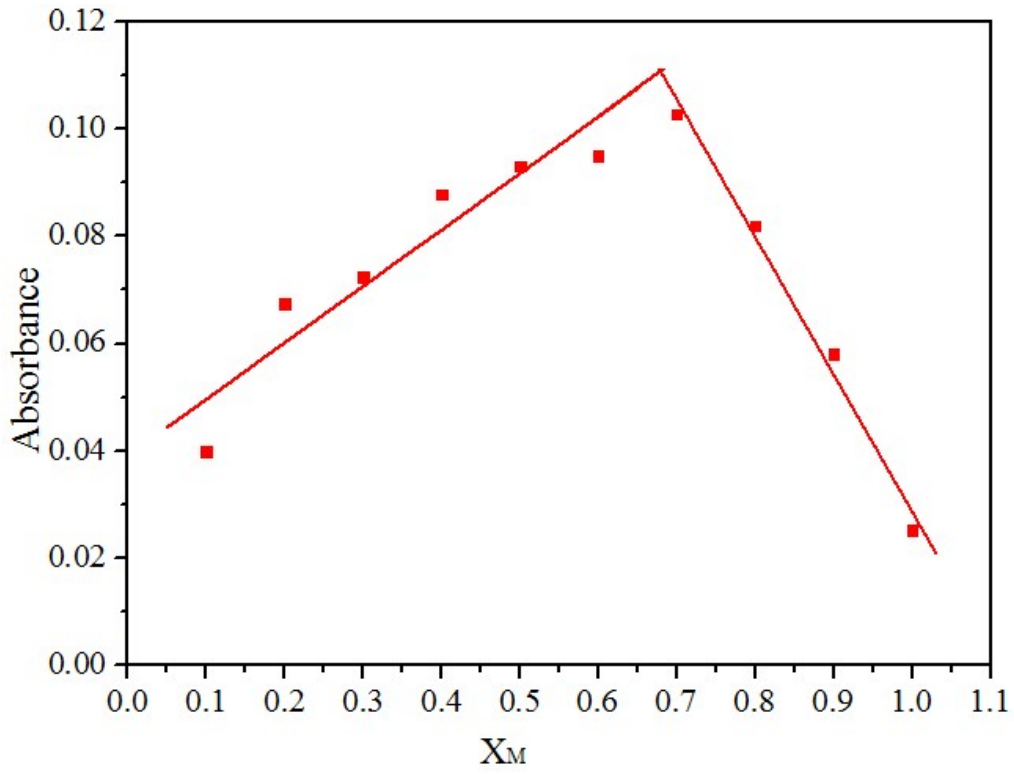

Figure S27. Absorbance spectral changes of stoichiometry calculations based on absorbance changes at 380 nm; X_M = $[Hg^{2+}]/([Hg^{2+}]+[A1])$; where X_M = mole fraction, $[Hg^{2+}]$ and [A1] are concentrations of Hg^{2+} and A1; A1+Hg^{2+} = 2:1 stoichiometry (ca. 0.66).

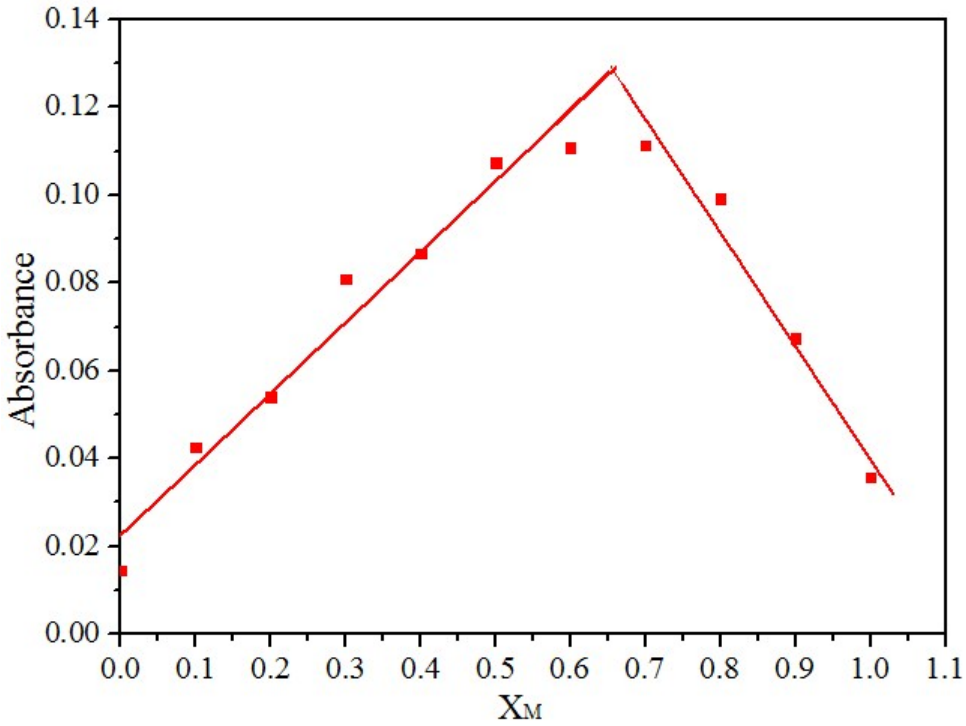

Figure S28. Absorbance spectral changes of stoichiometry calculations based on absorbance changes at 430 nm; X_M = $[Hg^{2+}]/([Hg^{2+}]$ +[A2]); where X_M = mole fraction, $[Hg^{2+}]$ and [A2] are concentrations of Hg^{2+} and A2; A2+Hg^{2+} = 2:1 stoichiometry (ca. 0.66).

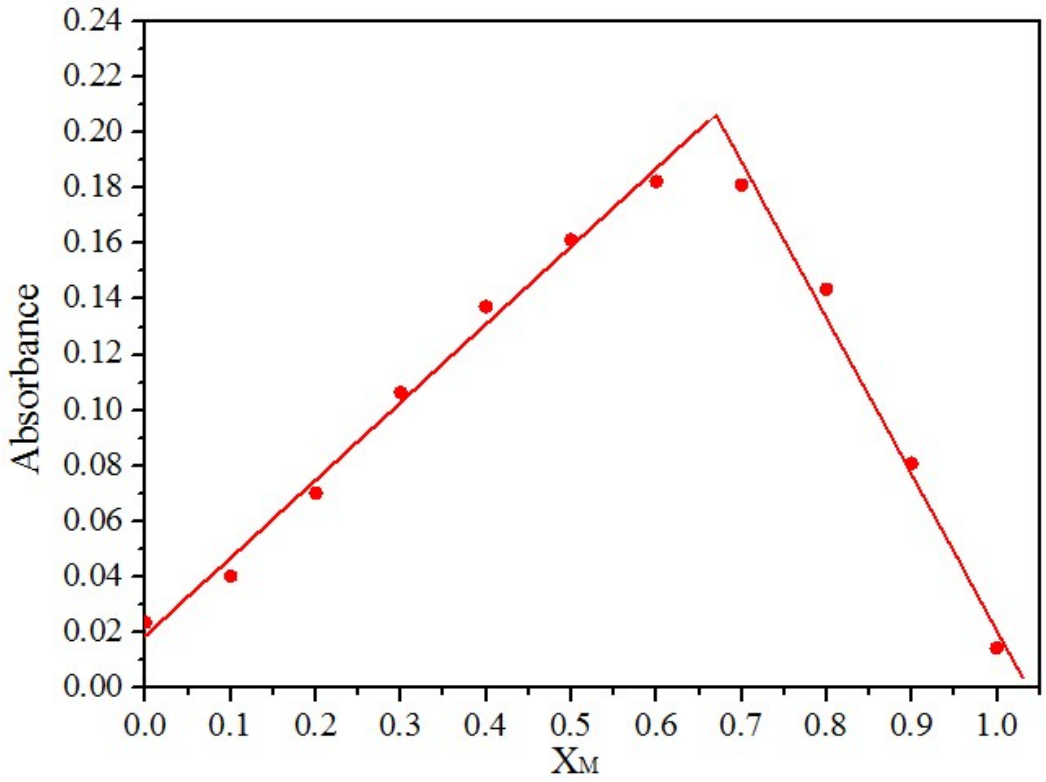

Figure S29. Absorbance spectral changes of stoichiometry calculations based on absorbance changes at 405 nm; X_M = $[Hg^{2+}]/([Hg^{2+}]$ +[A3]); where X_M = mole fraction, $[Hg^{2+}]$ and [A3] are concentrations of Hg^{2+} and A3; A3+Hg^{2+} = 2:1 stoichiometry (ca. 0.66).

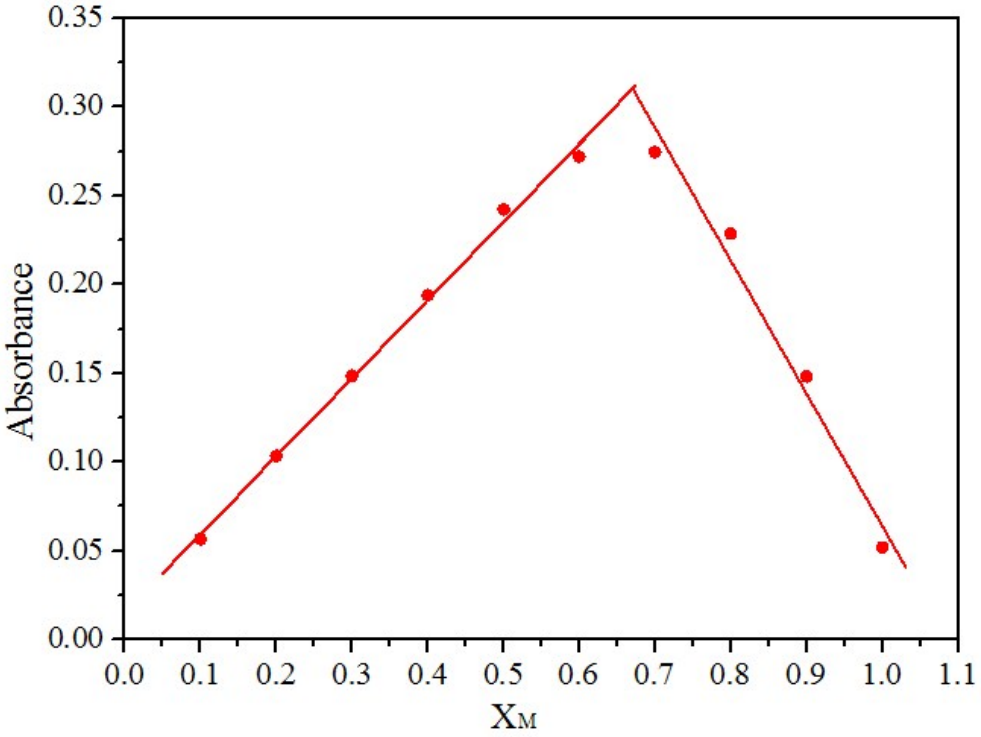

Figure S30. Absorbance spectral changes of stoichiometry calculations based on absorbance changes at 450 nm; X_M = $[Hg^{2+}]/([Hg^{2+}]+[A5])$; where X_M = mole fraction, $[Hg^{2+}]$ and [A5] are concentrations of Hg^{2+} and A5; A5+Hg^{2+} = 2:1 stoichiometry (ca. 0.66).

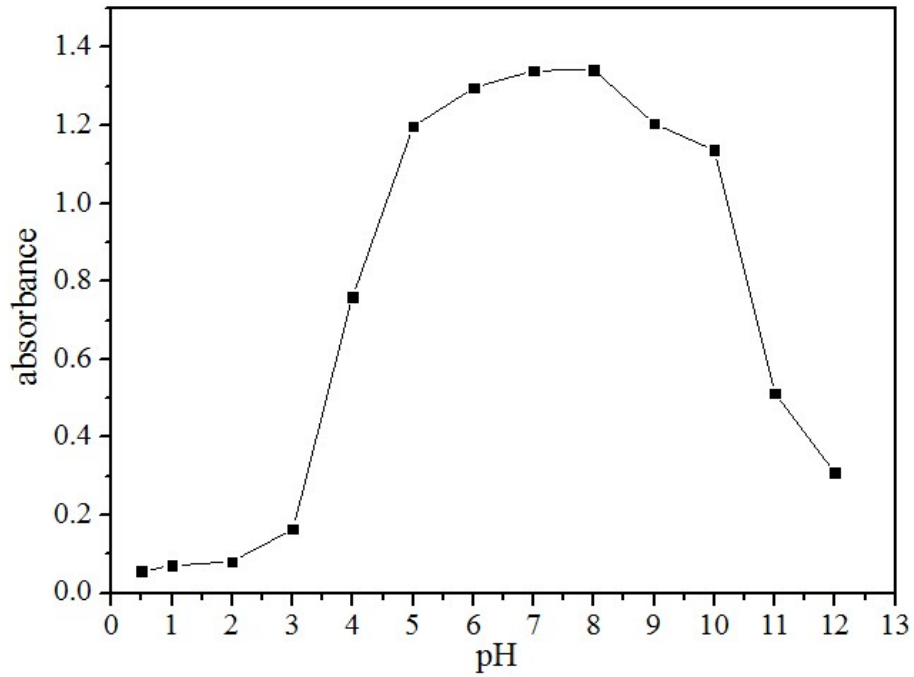

Figure S31**.** Shows that **A1** is stable within a wide pH range of 5.0–10.0, and the following tests are in the range of pH.

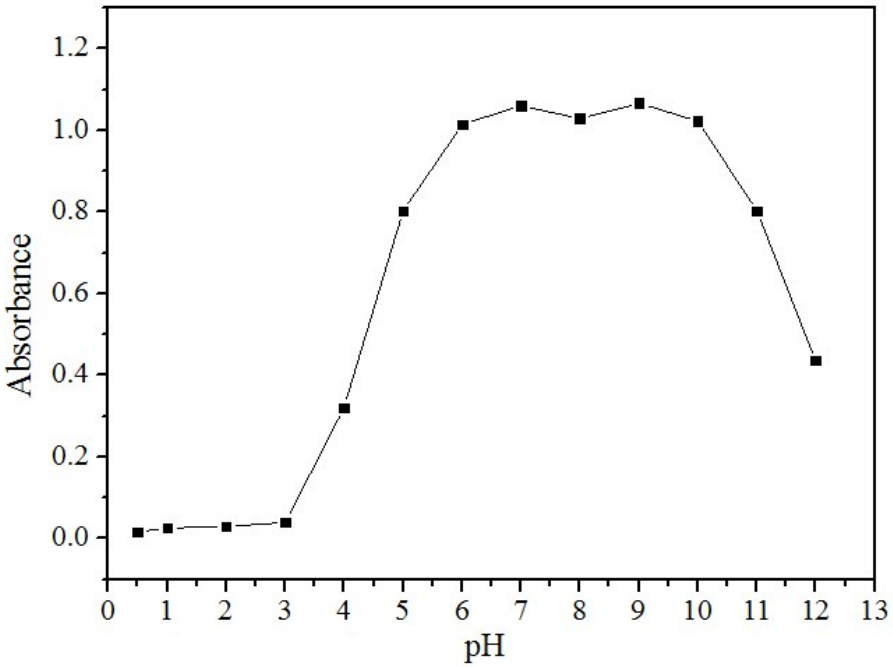

Figure S32. The stable range of pH values on **A3**, chemosensor **A3** (1.0×10^{-5} M) was added in 1.0 mL EtOH/H_2O solution (v/v = 4:1, 20 mM buffer). The buffers were: pH 1.0–2.0, HCl; pH 2.5–4.0, KHP/HCl; pH 4.5–6.0, KHP/NaOH; pH 6.5–10.0 Hepes/NaOH, pH 11.0–12.0 NaOH.

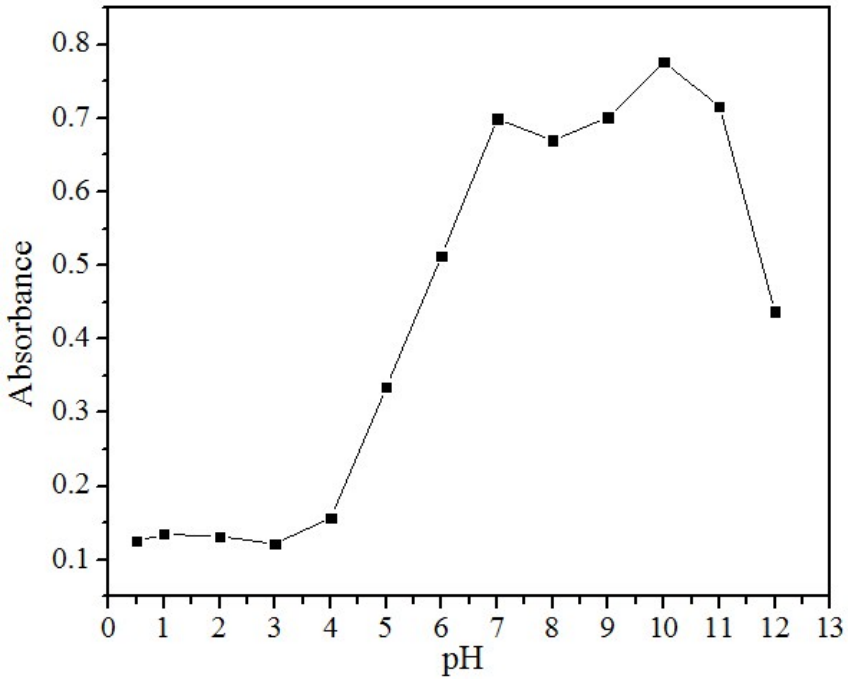

Figure S33. The stable range of pH values on **A5**, chemosensor **A5** (1.0×10^{-5} M) was added in 1.0 mL EtOH/H_2O solution (v/v = 2 : 1, 20 mM buffer). The buffers were: pH 1.0–2.0, HCl; pH 2.5–4.0, KHP/HCl; pH 4.5–6.0, KHP/NaOH; pH 6.5–10.0 Hepes/NaOH, pH 11.0–12.0 NaOH.

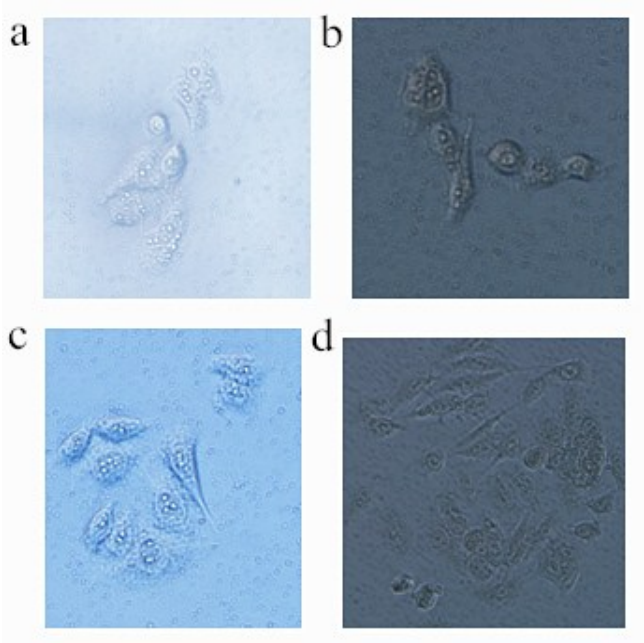

Figure S34. (a) Light micrograph of PC3 celluar treated with **A1**. (b) Light micrograph of PC3 celluar treated with **A1** and Hg^{2+}. (c) Light micrograph of PC3 celluar treated with **A2**. (d) Light micrograph of PC3 celluar treated with **A2** and Hg^{2+}.

Table S1

The UV–vis absorption data of ligands **A1**–**A5** and complexes **B1**–**B5**.

Ligands	λ1	λ2	Complexes	λ1	λ2
A1	257	362	**B1**	262	392
A2	245	364	**B2**	245	375
A3	263	365	**B3**	272	399
A4	279	377	**B4**	288	382
A5	287	343	**B5**	295	449